The 2015 World Congress on
Advances in Civil, Environmental, and Materials Research (ACEM15)
Incheon, Korea, August 25-29, 2015

The Variant Identification in Molecular Dynamics Simulations for Shape Memory Alloys

Jo-Fan Wu[1)], Chia-Wei Yang[2)], Chuin-Shan Chen[3)], *Nien-Ti Tsou[4)]

[1), 3)] *Department of Civil Engineering, National Taiwan University, No. 1, Sec. 4, Roosevelt Road, Taipei 10617, Taiwan*
[2), 4)] *Department of Materials Science and Engineering, National Chiao Tung University, Ta Hsueh Road, HsinChu 300, Taiwan*
[4)] tsounienti@nctu.edu.tw

ABSTRACT

Shape memory alloys (SMAs) have significant phenomena, such as superelasticity and shape memory effect, due to the phase transformation. These phenomena are dominated by the microstructures. Recently, the microstructures in SMAs have been extensively studied and modeled by using molecular dynamics (MD). However, it is difficult to identify the crystal variants in the simulation results which consist of large amount of atoms. In the present work, an algorithm is implemented to identify the austenite parent phase and the martensite crystal variants in the microstructure generated by MD. It examines the transformation matrix of the lattices, and determines the corresponding crystal variants. We apply the method to obtain the evolution of the volume fraction of the crystal variants in the monoclinic SMAs under thermal cycles. The method is verified and is particular useful for the post-processing of the MD simulations.

1. INTRODUCTION

Shape memory alloys (SMAs) are one of the most popular functional materials, which are extensively used in many important technological applications, including stents and actuators. This is because of their significant properties, such as superelasticity and shape memory effect. Among the various types of SMAs, the nickel titanium (Ni-Ti) is the most common alloy in the industry due to their biocompatibility, ductility, resistance to corrosion and good mechanical properties (Fernandes, Peres et al. 2011). These mechanical properties are dominated by the microstructure. For example, Saburi et al. (Hane and Shield 1999) found that the Ni-Ti single crystals do

---

[1)] Graduate Student
[2)] Assistant Professor
[3)] Graduate Student
[4)] Professor

not show the superelasticity behavior at any temperature. By contrast, the polycrystalline specimens with the fine grain size do have superelasticity response (Miyazaki, Ohmi et al. 1982). (Liu 2001) also found that the twin and detwinned microstructures play important roles in the level of the shape recovery. However, the microstructures during the phase transformation is difficult to be observed in experiments.

In order to reveal the detail of the microscopic behavior of Ni–Ti alloys, many numerical models have been developed recently. (Zhong and Zhu 2014) studied the dynamic microstructure evolution in SMAs by using phase-field method. (Kastner, Eggeler et al. 2011) used molecular dynamics (MD) method to simulate the non-diffusive nucleation and growth processes of martensite phase giving distinct microstructures. (Sato, Saitoh et al. 2006) revealed the microscopic mechanism of stress-induced martensitic transformation with the MD simulations. There are several studies (Kastner, Eggeler et al. 2011, Mirzaeifar, Gall et al. 2014) adopt the crystallographic theory to identify martensite crystal variants in their atomistic model. However, the limited set of present crystal variants are typically assumed and thus the analysis of the microstructure may not be complete. This motivates the current study to develop a numerical procedure to identify the full set of crystal variants in the atomistic model without prior assumptions.

In this paper, the microstructure evolution between austenite phase and martensite phase in Ni-Ti SMAs is modeled by MD. Then a numerical method is developed to analyze the position of atoms and to examine the transformation matrix of the unit cells. This allows us to identify the austenite parent phase and the martensite crystal variants in the microstructures without ambiguity. Thus, the transition between the cubic and the monoclinic crystal systems can be revealed. The method of crystal variant identification is rapid and complete without the prior assumptions. This enables an efficient exploration for martensitic microstructures, and allow a full understanding to the phase transformation in SMAs.

2. THEORY AND METHODOLOGY

2.1 Martensitic transformation

In this paper, we consider the phase transition in Ni-Ti SMAs, which is corresponding to the cubic to monoclinic crystal system. Fig. 1(a) (Bhattacharya 2003) shows the lattice structure of the austenite parent phase with four cubic unit cells, which can also be represented by a tetragonal unit cell marked in dashed lines. After the martensitic phase transition, the tetragonal unit cell is then distorted, resulting in a unit cell with length a, b, c and a non 90° angle β between two edges *a* and *c*, as shown in Fig. 1(b). It is also worth noting that the monoclinic unit cell is similar to a face-centered cell with a plane of atoms shifted from its natural positions.

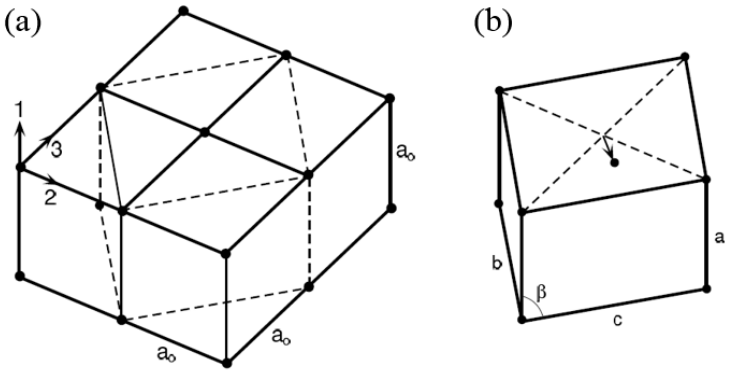

Fig. 1 The martensitic transformation in Ni-Ti alloy (Only the Ti atoms are shown): (a) the cubic unit cells and a tetragonal unit cell marked with dashed line; (b) the monoclinic unit cell of martensite (Bhattacharya 2003).

There are 12 types of the unit cell distortion for the cubic to monoclinic phase transformation. They are the so-called crystal variants. Here the distortion of the unit cells is assume to be homogeneous, and can be described by the transformation matrices $\boldsymbol{U}_m$ $(m=1\ldots12)$, given by

$$\boldsymbol{U}_1=\begin{pmatrix}\gamma & \varepsilon & \varepsilon\\ \varepsilon & \alpha & \delta\\ \varepsilon & \delta & \alpha\end{pmatrix},\qquad \boldsymbol{U}_2=\begin{pmatrix}\gamma & -\varepsilon & -\varepsilon\\ -\varepsilon & \alpha & \delta\\ -\varepsilon & \delta & \alpha\end{pmatrix};$$

$$\boldsymbol{U}_3=\begin{pmatrix}\gamma & -\varepsilon & \varepsilon\\ -\varepsilon & \alpha & -\delta\\ \varepsilon & -\delta & \alpha\end{pmatrix},\quad \boldsymbol{U}_4=\begin{pmatrix}\gamma & \varepsilon & -\varepsilon\\ \varepsilon & \alpha & -\delta\\ -\varepsilon & -\delta & \alpha\end{pmatrix};$$

$$\boldsymbol{U}_5=\begin{pmatrix}\alpha & \varepsilon & \delta\\ \varepsilon & \gamma & \varepsilon\\ \delta & \varepsilon & \alpha\end{pmatrix},\qquad \boldsymbol{U}_6=\begin{pmatrix}\alpha & -\varepsilon & \delta\\ -\varepsilon & \gamma & -\varepsilon\\ \delta & -\varepsilon & \alpha\end{pmatrix};$$

$$\boldsymbol{U}_7=\begin{pmatrix}\alpha & -\varepsilon & -\delta\\ -\varepsilon & \gamma & \varepsilon\\ -\delta & \varepsilon & \alpha\end{pmatrix},\quad \boldsymbol{U}_8=\begin{pmatrix}\alpha & \varepsilon & -\delta\\ \varepsilon & \gamma & -\varepsilon\\ -\delta & -\varepsilon & \alpha\end{pmatrix};$$

$$\boldsymbol{U}_9=\begin{pmatrix}\alpha & \delta & \varepsilon\\ \delta & \alpha & \varepsilon\\ \varepsilon & \varepsilon & \gamma\end{pmatrix},\qquad \boldsymbol{U}_{10}=\begin{pmatrix}\alpha & \delta & -\varepsilon\\ \delta & \alpha & -\varepsilon\\ -\varepsilon & -\varepsilon & \gamma\end{pmatrix};$$

$$\boldsymbol{U}_{11}=\begin{pmatrix}\alpha & -\delta & \varepsilon\\ -\delta & \alpha & -\varepsilon\\ \varepsilon & -\varepsilon & \gamma\end{pmatrix},\quad \boldsymbol{U}_{12}=\begin{pmatrix}\alpha & -\delta & -\varepsilon\\ -\delta & \alpha & \varepsilon\\ -\varepsilon & \varepsilon & \gamma\end{pmatrix}. \tag{1}$$

where the components can be written in the form of the lattice parameters $a_0,\ a,\ b,\ c$ and β

$$\begin{aligned}
\gamma &= \frac{a\left(\sqrt{2}a + c\sin\beta\right)}{a_0\sqrt{2a^2 + c^2 + 2\sqrt{2}ac\sin\beta}},\\
\varepsilon &= \frac{ac\cos\beta}{\sqrt{2}a_0\sqrt{2a^2 + c^2 + 2\sqrt{2}ac\sin\beta}},\\
\alpha &= \frac{1}{2\sqrt{2}a_0}\left(\frac{c\left(c + \sqrt{2}a\sin\beta\right)}{\sqrt{2a^2 + c^2 + 2\sqrt{2}ac\sin\beta}} + b\right),\\
\delta &= \frac{1}{2\sqrt{2}a_0}\left(\frac{c\left(c + \sqrt{2}a\sin\beta\right)}{\sqrt{2a^2 + c^2 + 2\sqrt{2}ac\sin\beta}} - b\right).
\end{aligned} \tag{2}$$

The transformation matrices mentioned above describe the distortion of the unit cells as well as the displacement of the atom position. Thus, they can be the references for the crystal variant identification in the microstructures generated by MD.

2.2 Interatomic potential and molecular dynamics modeling

In this work, a Finnis-Sinclair (FS) type many-body interatomic potential (Finnis and Sinclair 1984) with embedded atom method (EAM) is adopted for describing the Ni-Ti system. This binary potential was formerly constructed by (Lai and Liu 2000) and then further improved by (Zhong, Gall et al. 2011) with a modified smooth interpolations around the cutoff radius. This allows an accurate and efficient prediction on the lattice constants and energies of different phases compared to the *ab initio* calculations

In the current study, the MD simulations of thermo-induced martensite transformation is performed by LAMMPS (Plimpton 1995). A single-crystal B2 structure consisted of 65,536 atoms is initialized based on the cubic parent coordinate. The entire structure is 9.63 nm long on each side. The periodic boundary condition is applied in the three directions for bulk modelling. After the energy minimization, the simulation temperature is set to 450 K, about 100 K higher than the austenite finish temperature A_f (~350 K). The system is then cooled down instantly to 100 K, about 190 K lower than the martensite finish temperature M_f (~290 K). At each of the both temperature stages, the structure is relaxed at zero stress for 60,000 MD time steps (0.5 fs per step) for thermal equilibration.

2.3 Structural analysis method for the identification of monoclinic martensite variants and austenite

We now consider the atom arrangement right after the energy minimization as the reference configuration in B2 structure for computing a_0 and deformation matrices. Then, a separate small size MD calculation is performed to form a pure monoclinic martensite variant. By examining the position of the atoms, a set of mean lattice parameters $(a,\ b,\ c,\ \beta)$ can be determined. This leads that the values

$(\alpha,\ \gamma,\ \delta,\ \varepsilon) = (1.0003,\ 0.9978,\ -0.0046,\ -0.0238)$ in Eq. (2). Thus, by substituting $(\alpha,\ \gamma,\ \delta,\ \varepsilon)$ into Eq. (1), the standard table of monoclinic transformation matrices in the current MD calculation can be found.

Now we are ready to examine the monoclinic variants in the entire structure by extracting the transformation matrix of lattices. Here, a method for calculating the transformation matrix of a single lattice by examining the local atom positions is used (Shimizu, Ogata et al. 2007). Consider a deformation gradient $\boldsymbol{F}_i$ for each lattice *i* which maps

$$\left\{\boldsymbol{d}_j^0\right\} \to \left\{\boldsymbol{d}_j\right\}, \forall j \in N_i^0 \tag{3}$$

where $\boldsymbol{d}_j$ are the vector from the lattice center pointing to *j*th Ti atom which occupies one of the 8 corners of the lattice *i* (the superscript 0 here indicates the reference configuration). Then, the deformation gradient $\boldsymbol{F}_i$ can be determined by minimizing the following equation:

$$\sum_{j \in N_i^0} \left| \boldsymbol{d}_j^0 \boldsymbol{F}_i - \boldsymbol{d}_j \right|^2 \tag{4}$$

Based on the polar decomposition theorem, when $det\,\boldsymbol{F} > 0$, the deformation gradient $\boldsymbol{F}$ can be written as $\boldsymbol{F} = \boldsymbol{R}\boldsymbol{U}$. Where $\boldsymbol{R}$ is a rotation matrix; $\boldsymbol{U}$ is a positive-definite symmetric matrix, i.e. transformation matrix, such that $\boldsymbol{U} = \sqrt{\boldsymbol{F}^T \boldsymbol{F}}$ (Hane and Shield 1999). Note that these transformation matrices are not corresponding to the previous cubic basis but the deformed coordinate, and thus, an appropriate rotation for the coordinates is needed.

We now analyze the B19' monoclinic variants in the structures. The simulation box is firstly divided into sets of the super cells consisted of 8 parent unitcells as illustrated in Fig. 2(a). The transformation matrix of the six tetragonal unit cells with the rotated coordinate (colored lines in Fig. 2(b) ~ (d)) in the super cell can be determined. Each transformation matrices is the possible candidate of the variants in the super cell. The error $\boldsymbol{\sigma}_m$ between each transformation matrix and each the standard monoclinic transformation matrices is obtained by

$$\boldsymbol{\sigma}_m = \sum_{j=1}^{3} \sum_{k=j}^{3} \left(\boldsymbol{U}_{jk}^i - \boldsymbol{U}_{jk}^m \right)^2, \forall m = 1 \sim 13 \tag{5}$$

where *i* denotes the lattice number, $m = 1 \sim 12$ stands for the 12 standard transformation matrices and $m = 13$ for non-deformed lattice, i.e. austenite parent phase. The crystal variant of the super cell can then be regarded as the candidate with the lowest error. Note that the perturbation of atoms during simulation is eliminated by applying ensemble average method.

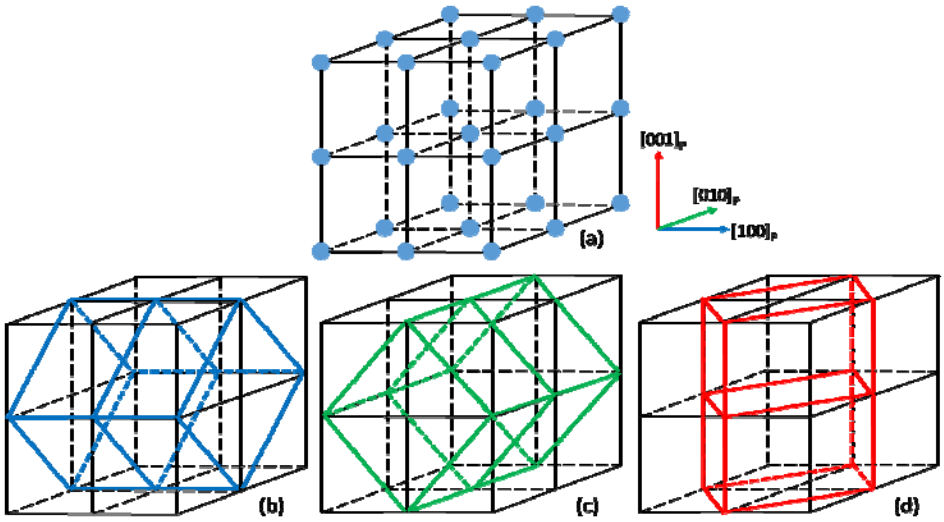

Fig. 2 A super cell which is formed by 8 adjacent unit cells. (a) here only Ti atoms are shown as blue circles for clarity. Two tetragonal cell with short axis lying on (b) $[100]_P$, (c) $[010]_P$, and (d) $[001]_P$ directions.

3. PHASE TRANSITION BETWEEN B2 AND B19' IN BULK NITI

The method provided in the previous section is now applied to identify the variants evolution in the temperature-driven phase transition. The results are shown in Figs. 3 and 4. In Fig. 3, the volume fraction of austenite decreases significantly because of the immediate drop of the temperature from 450K to 100K. On the contrast, four variants (1, 2, 11, and 12) grow rapidly. Then the variant 1 dominates the crystal after 2 picoseconds. Note that the results show that the austenite phase remains and is located around the twinning interfaces even after 6 picoseconds.

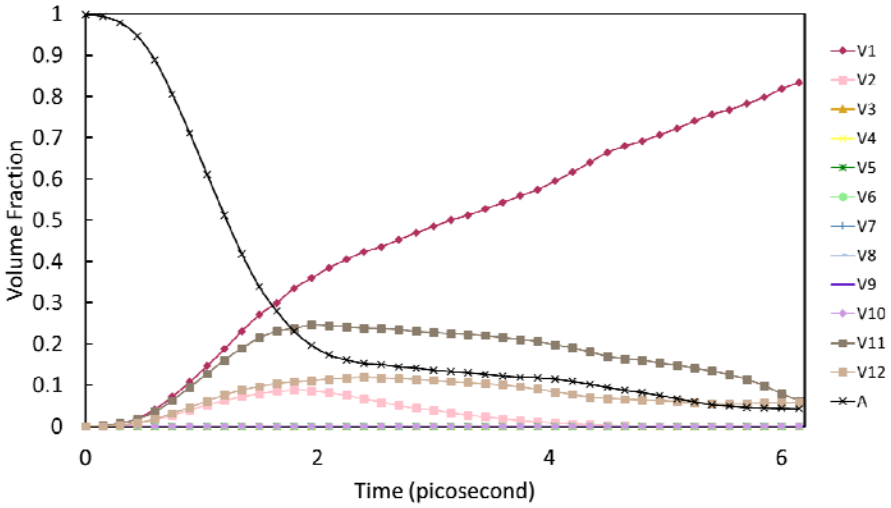

Fig. 3 Volume fraction variation of austenite parent phase and 12 monoclinic martensite variants during temperature-driven phase transformation.

The microstructure evolution is shown in Fig. 4. Fig. 4(a) shows the austenite phase in white color before temperature drops. Fig. 4(b) illustrates the microstructure evolution at 2 picoseconds, showing a complicated topology consisted of variants 1, 2, 11 and 12. Then, apart from variant 1, all the variants vanished progressively (Fig. 4(c)) until the end of the simulation, leaving a narrow band of the twinned-structure as shown in Fig. 4(d). Note that the result also shows that small amount of the austenite phase super cells remain and are located around the twinning interfaces even after 6 picoseconds, as shown in Fig. 4(d).

4. CONCLUSIONS

The present study proposed a post-processing method for identifying specific variants group in the molecular dynamics simulation based on the crystallographic theory. The method is applied to analyze the cubic to monoclinic phase transformation in the NiTi SMAs. The microstructure evolution during the phase transition is determined. The current method is ready to extend for different crystal systems and related materials, such as ferroelectrics.

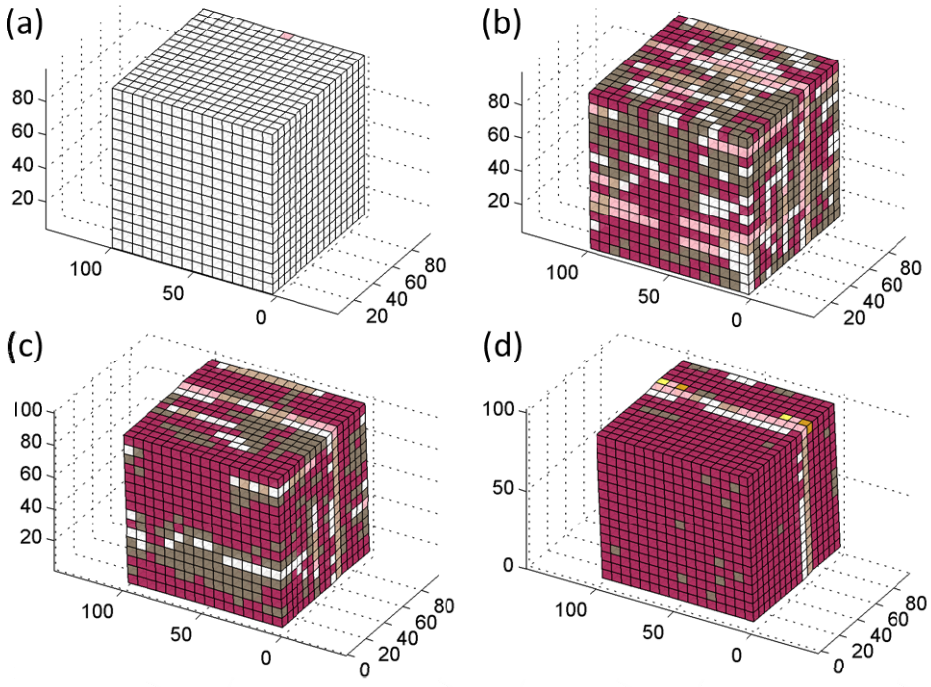

Fig. 4 Evolution of microstructure during phase transition: (a) start at 0 picosecond; (b) 2 picoseconds; (c) 4 picoseconds and; (d) 6 picoseconds after reducing temperature.

REFERENCES

Bhattacharya, K. (2003). *Microstructure of martensite: why it forms and how it gives rise to the shape-memory effect*, Oxford University Press.

Fernandes, D. J., Peres, R. V., Mendes, A. M. and Elias, C. N. (2011). "Understanding the shape-memory alloys used in orthodontics." *ISRN dentistry* **2011**.

Finnis, M. W. and Sinclair, J. E. (1984). "A Simple Empirical N-Body Potential for Transition-Metals." *Philos. Mag. A* **50**(1): 45-55.

Hane, K. F. and Shield, T. (1999). "Microstructure in the cubic to monoclinic transition in titanium–nickel shape memory alloys." *Acta Mater.* **47**(9): 2603-2617.

Kastner, O., Eggeler, G., Weiss, W. and Ackland, G. J. (2011). "Molecular dynamics simulation study of microstructure evolution during cyclic martensitic transformations." *J. Mech. Phys. Solids* **59**(9): 1888-1908.

Lai, W. S. and Liu, B. X. (2000). "Lattice stability of some Ni-Ti alloy phases versus their chemical composition and disordering." *J. Phys.: Condens. Matter* **12**(5): L53-L60.

Liu, Y. (2001). "Detwinning process and its anisotropy in shape memory alloys", *Smart Materials and MEMS*

Mirzaeifar, R., Gall, K., Zhu, T., Yavari, A. and DesRoches, R. (2014). "Structural transformations in NiTi shape memory alloy nanowires." *J. Appl. Phys.* **115**(19): 194307.

Miyazaki, S., Ohmi, Y., Otsuka, K. and Suzuki, Y. (1982). "Characteristics of Deformation and Transformation Pseudoelasticity in Ti-Ni Alloys." *J Phys-Paris* **43**(Nc-4): 255-260.

Plimpton, S. (1995). "Fast Parallel Algorithms for Short-Range Molecular-Dynamics." *J. Comput. Phys.* **117**(1): 1-19.

Sato, T., Saitoh, K.-i. and Shinke, N. (2006). "Molecular dynamics study on microscopic mechanism for phase transformation of Ni–Ti alloy." *Modelling Simul. Mater. Sci.* **14**(5): S39.

Shimizu, F., Ogata, S. and Li, J. (2007). "Theory of shear banding in metallic glasses and molecular dynamics calculations." *Mater. Trans., Jim* **48**(11): 2923-2927.

Zhong, Y., Gall, K. and Zhu, T. (2011). "Atomistic study of nanotwins in NiTi shape memory alloys." *J. Appl. Phys.* **110**(3): -.

Zhong, Y. and Zhu, T. (2014). "Phase-field modeling of martensitic microstructure in NiTi shape memory alloys." *Acta Mater.* **75**: 337-347.